Pertanika J. Sci. & Technol. 33 (6): 2747 - 2770 (2025)

PERTANIKA JOURNALS

SCIENCE & TECHNOLOGY

Journal homepage: http://www.pertanika.upm.edu.my/

Development and Verification of an MCNP5-based Gamma Camera for ^{177}Lu SPECT Imaging

Puvanesuawary Morthy[1], Marianie Musarudin[1]*, Nor Shazleen Ab Shukor[1], Mohamad Aminudin Said[2], Dong Xianling[3] and M. Iqbal Saripan[4]

[1]School of Health Sciences, Health Campus, Universiti Sains Malaysia, 16150 Kota Bharu, Kelantan, Malaysia
[2]Department of Nuclear Medicine, Institut Kanser Negara, 62250 Putrajaya, Wilayah Persekutuan Putrajaya, Malaysia
[3]Hebei International Research Center of Medical Engineering, Chengde Medical University, Chengde 067050, China
[4]Faculty of Engineering, Universiti Putra Malaysia, 43400 Serdang, Selangor, Malaysia

ABSTRACT

Monte Carlo (MC) simulations in single-photon emission computed tomography (SPECT) are invaluable for enhancing activity quantification in patients, thereby facilitating an accurate estimate of the absorbed dose for every organ. The validation of MC results against experimental data is essential to ensure their reliability. This study focuses on lutetium-177 (^{177}Lu) SPECT imaging modeling using the Monte Carlo N-Particle Transport, version 5 (MCNP5) code. The objective was to validate the MC code for ^{177}Lu SPECT by comparing simulated and experimental data on system sensitivity, image quality, intensity profiles, and energy resolution. The gamma camera was modeled based on the GE HealthCare Discovery nuclear medicine/computed tomography (NM/CT) 670 Pro, with a medium energy general purpose (MEGP) collimator. MC simulations accounted for the SPECT scanner's physical specifications, Gaussian energy blurring, and corrections for scatter and attenuation. Post-simulation analysis was performed in the Matrix Laboratory (MATLAB) software, with comparisons made under identical geometrical configurations for experimental and simulated data. The results revealed a strong agreement between simulated and experimental data. System sensitivities varied by only 3.34%, while the structural similarity index metric (SSIM) value of 0.9348 demonstrated a high level of similarity. The energy resolutions for 113 and 208 keV were 16.28 and 15.69%, respectively. Additionally, high correlation coefficients across spheres further validated the accuracy of the MC model. These remarkable agreements confirm the accuracy and precision of the MCNP5-based

ARTICLE INFO

Article history:
Received: 28 March 2025
Accepted: 16 July 2025
Published: 14 October 2025

DOI: https://doi.org/10.47836/pjst.33.6.15

E-mail addresses:
puvanesmorthy0698@gmail.com (Puvanesuawary Morthy)
marianie@usm.my (Marianie Musarudin)
shazzleen@usm.my (Nor Shazleen Ab Shukor)
aminhpj@gmail.com (Mohamad Aminudin Said)
dongxl_cdmc@163.com (Dong Xianling)
iqbal@upm.edu.my (M. Iqbal Saripan)
* Corresponding author

e-ISSN: 2231-8526

^{177}Lu SPECT imaging simulations. In conclusion, the validated MCNP5 model of the gamma camera provides a foundation for future research into ^{177}Lu SPECT imaging and quantification.

Keywords: ^{177}Lu, Monte Carlo, SPECT, verification

INTRODUCTION

SPECT is now widely recognized as a key tool in nuclear medicine research for the localization of *in vivo* radiopharmaceuticals, as it can generate three-dimensional images (Bouchareb et al., 2024). Through detecting gamma photons emitted from radiopharmaceuticals and their reconstruction into tomographic images, SPECT offers crucial insights into the physiological functions of organs and tissues that other imaging modalities often do not provide (Mishra, 2024). This modality is widely utilized in oncology, cardiology, and neurology, where an accurate quantitative assessment of radioactivity in tissues is vital for effective diagnosis, treatment, and dosimetry evaluation. The combination of SPECT with computed tomography (CT) has led to the development of non-invasive hybrid SPECT/CT clinical systems, which have improved clinical applications by integrating anatomical (CT) and functional (SPECT) imaging, resulting in widespread adoption globally since 1999 (Zaidi, 1999). These systems play a crucial role in cancer diagnosis and treatment, enhancing the accuracy and precision of radiotherapy planning (Seo et al., 2008). However, the effectiveness of SPECT imaging is heavily dependent on the performance of the gamma camera.

In recent years, MC simulations have become increasingly important for assessing and optimizing gamma camera performance. MC models are frequently employed across various nuclear medicine modalities to refine imaging protocols, evaluate collimator designs, and improve quantitative accuracy (Dong et al., 2018; Musarudin et al., 2015; Ramonaheng et al., 2020; Saripan et al., 2009). Validating an MC model is mandatory before using it to simulate a SPECT imaging system. Due to the approximations and simplifications inherent in the physics laws formulated within an MC code (Di Domenico et al., 2023), validation is important to ensure accuracy between simulated and experimental measurements across key parameters. This comparison not only identifies discrepancies but also helps refine the MC model for improved accuracy.

Various MC codes, including MCNP, simulating medical imaging nuclear detectors (SIMIND) and GEometry ANd Tracking 4 (GEANT4), have been extensively utilized to model gamma cameras for SPECT imaging, with numerous studies confirming their accuracy and reliability. For instance, Bahnamiri et al. (2015) used MCNP calculations to explore the effect of collimator parameters on SPECT image quality and discovered a relative difference of less than 5% between simulation and experimental data, validating the accuracy of the simulation. Recently, Di Domenico et al. (2023) demonstrated that the

SIMIND MC code for gamma camera modeling is effective in simulating both planar and SPECT gamma camera systems for optimal quantification by validating calibration factors (CF) and recovery coefficients (RC) derived using this code. Similarly, Pells et al. (2023) explored simulation and experimental uncertainties in the spatial resolution, sensitivity, energy spectra, and projection images using the GEANT4 Application for Tomographic Emission (GATE) toolkit. Bui et al. (2023) evaluated the performance of the GEANT4-based MC model of a SPECT scanner in terms of detection efficiency, spatial resolution, and activity RC, achieving good agreement between the simulated and experimental data. Collectively, these studies demonstrate the ability of MC simulations to accurately model key parameters, such as the collimator influence, CF, RC, spatial resolution, and detection efficiency. The close match between the simulated and experimental data highlights the potential of MC models to improve SPECT quantification and image quality, emphasizing their role in advancing the accuracy and effectiveness of SPECT imaging systems.

Researchers typically validate simulations of nuclear imaging modalities by examining various parameters, including the spatial resolution, planar sensitivity, CF, and RC for isotopes like technetium-99m (^{99m}Tc), ^{177}Lu, and iodine-131 (^{131}I) (Bahreyni Toossi et al., 2010; Dong et al., 2018; Ejeh et al., 2019; Ramonaheng et al., 2020). These parameters offer valuable insights into the performance of MC codes in modeling gamma cameras, ensuring their effectiveness for future clinical applications (Morphis et al., 2021). ^{177}Lu has emerged as a promising radionuclide for targeted radionuclide therapy, namely in the treatment of neuroendocrine tumors and prostate cancer (Bodei et al., 2011; Ezziddin et al., 2014; Ilan et al., 2015; Paganelli et al., 2014; Romer et al., 2014; van der Zwan et al., 2015). With its favorable decay characteristics, beta emissions for therapy, and gamma emissions at 113 and 208 keV for imaging, ^{177}Lu has become a key radionuclide in theranostic applications, highlighting the necessity for precise SPECT quantification of ^{177}Lu in patient studies.

While MC simulations hold promise for optimizing SPECT imaging, accurately modeling complex clinical systems for quantitative analysis remains challenging. This study aims to develop and evaluate an MC-modeled gamma camera for Discovery NM/CT 670 Pro using the MCNP5 with ^{177}Lu. In our previous study, a simulation framework based on MNCP5 was successfully introduced to derive CFs and RCs for ^{177}Lu quantification, but it only offered a preliminary verification of the gamma camera model (Morthy et al., 2025). A comprehensive, system-wide validation that is essential for establishing the accuracy and precision of the model was not thoroughly explored. Notably, key performance metrics such as qualitative and quantitative image quality, sphere-wise intensity profiles, full width at half maximum (FWHM) analysis, and energy resolution were not systematically assessed. The current study addresses these gaps by performing a rigorous, multidimensional validation of an MCNP5 model meticulously tailored to the GE Discovery NM/CT 670 Pro gamma camera equipped with a MEGP collimator for ^{177}Lu SPECT imaging. This validation

includes thorough comparisons with experimental data to ensure high spatial, structural, and energy fidelity in the simulation. The enhanced agreement between simulation and experimental data significantly improves the MC model's reliability for future applications in personalized dosimetry, protocol optimization, and quantitative SPECT research. By enhancing MCNP5 for SPECT scanner simulation, this research seeks to improve imaging protocols and aid the development of innovative reconstruction algorithms.

MATERIALS AND METHODS

This research was divided into three phases: system sensitivity measurement, National Electrical Manufacturers Association (NEMA) phantom SPECT imaging and MC simulation, and verification of the MC-modeled gamma camera. The first phase involved assessing the system's ability to detect the incident photons and establishing baseline sensitivity data. In the second phase, a NEMA phantom was scanned using a SPECT system, while a corresponding MC simulation was run to model the SPECT imaging process. The acquisition and reconstruction settings determined using the GE Discovery NM/CT 670 Pro SPECT system in the previous study by Morthy (2025) were applied to both the experimental and simulation SPECT systems in this study. A compromise between the optimal image quality and quantification accuracy was achieved by employing the MEGP collimator, a slice thickness of 5 mm, and a reconstruction algorithm employing ordered subset expectation maximization (OSEM), where two iterations and 10 subsets constituted the optimal approach (Morthy, 2025). Dead time effects were considered negligible for the data acquired in this study, as they were estimated to be only a few percent based on previous studies (Nakanishi et al., 2024). The third phase aimed to verify the accuracy of the MC-modeled gamma camera by comparing simulated and experimental data. A 10% uncertainty was considered sufficient for the objectives of this study, with the simulation likely converging with the targeted 68% confidence interval. Table 1 summarizes key characteristics of ^{177}Lu, including its half-life, primary gamma radiation emissions, and maximum energy of its beta radiation emissions.

Table 1
Physical properties of a lutetium-177 (^{177}Lu) radioisotope

Radionuclide	Half-life ($t_{1/2}$, days)	Strongest γ emission Eγ (keV) (Iγ [%])	Maximum β energy (Emax, keV)
^{177}Lu	6.65	112.9 (6.2) 208.4 (10.4)	498.3

Source: Asmi et al. (2020)

System Sensitivity

Sensitivity refers to the probability that a photon will be detected by the imaging system, directly reflecting its efficiency in capturing incident radiation. To evaluate system sensitivity, planar imaging was performed using both simulation and experimental setups, where Petri dishes (d = 9 cm) were placed directly on top of the detector head, as depicted in Figure 1. Each setup contained ^{177}Lu activity concentration of 5.36 ± 0.17 MBq/ml. For the simulation configuration in MCNP5, 2.68 × 10^8 photons were simulated to replicate the same activity scanned, calculated using Equation 1:

$$n_{photons} = C \times v \times t \times (P_{113} + P_{208}) \quad [1]$$

where C is the activity concentration (5.36 ± 0.17 MBq/ml), v is the volume of the radioactive solution (20 ml), t is the acquisition time (15 s), and P_{113} and P_{208} are the emission probabilities of photons per decay for 113 and 208 keV, respectively. The experimental setup acquired planar images using a 128 × 128 image matrix with a pixel resolution of 4.42 × 4.42 mm^2.

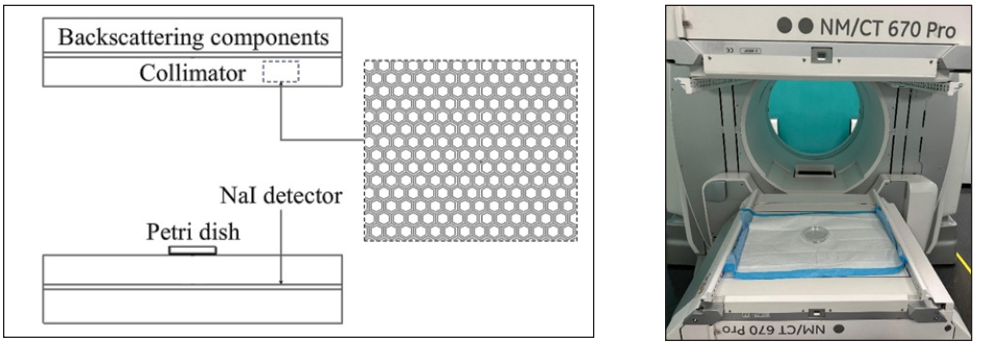

(a) (b)

Figure 1. Planar imaging configuration of the Petri dish: (a) simulation conducted using the MCNP5 code, and (b) experimental imaging performed using the GE Discovery NM/CT 670 Pro system
Note. NaI = Sodium iodide; MCNP5 = Monte Carlo N-particle Transport, version 5; NM/CT = Nuclear medicine/computed tomography

The first component, the collimator, consists of a slab featuring hexagonal holes and lead-filled septa (Figure 1a). The next component is a detector containing sodium iodide (NaI) with a 3.67 g/cm^3 density. The following are the backscattering components, modeled using a Pyrex block measuring 6.6 cm with a density of 66% of the standard Pyrex value of 1.47 g/cm^3 (De Vries et al., 1990). This setup simulates backscattering effects from the components located behind the detector, namely, light pipe, photomultiplier tubes (PMTs), mu-metal magnetic shielding, or other structural components in an actual camera (De Vries

et al., 1990), with a particular emphasis on the impact of PMT. The surfaces and cells of the MC model were defined using the repeated structure card in MCNP5. The parameters of the MC-modeled gamma camera, as specified in the GE data sheet, are provided in Table 2. To build the MC model as realistically as possible, MCNP5 and MATLAB software were combined to achieve comparable performance to the GE HealthCare Discovery NM/CT 670 Pro.

Table 2
GE HealthCare Discovery NM/CT 670 Pro specifications (GE HealthCare, n.d.)

System parameters	Data
Collimator	MEGP
Type of collimator	Parallel hole collimator
Hole shape	Hexagonal
Hole diameter	3.0 mm
Septal thickness	1.05 mm
Hole length	58 mm
Collimator field-of-view	54 cm × 40 cm
Thickness of the crystal	9.5 mm
Total number of PMTs	59 [53 (76 mm) and 6 (38 mm)]
PMT array	Hexagonal

Note. NM/CT = Nuclear medicine/computed tomography; MEGP = Medium energy general purpose; PMT = Photomultiplier tube

As indicated in Equation 2, the decay-corrected count rate, which was derived from the sum of counts over the entire image for the corresponding acquisition time per activity as recorded in the dose calibrator, was used to compute the experimental system sensitivity (Ramonaheng et al., 2020).

$$System\ sensitivity = \frac{Count\ rate\ (cps)}{Activity\ (MBq)} \quad [2]$$

Following the approach of Morthy et al. (2025), a similar calculation was performed to determine the simulated system sensitivity. The proportionality constant, k (Bq/counts), was adopted to convert pixel values into counts, as indicated in Equation 3. Here, A represents the activity measured in Bq, while CTS denotes the total counts extracted from the energy spectrum. The pixel-wise count values in the image were then calculated by multiplying the pixel values by this constant. This method assumes a direct proportionality between activity and counts within the system's linear range. Additionally, a region of interest was defined at the center of the image to exclude edge effects (D'Arienzo et al., 2016).

$$k = \frac{A}{\sum CTS} \quad [3]$$

A comprehensive approach to model validation was provided by comparing experimental and simulated data using Pearson's correlation and Lin's concordance correlation coefficient (CCC) to assess the accuracy of the MC-modeled gamma camera.

SPECT Imaging Using Discovery NM/CT 670 Pro

A static positron emission tomography (PET) NEMA phantom (NEMA 2007/IEC 2008, Phantom Laboratory, USA) was employed for SPECT imaging using the SPECT/CT imaging system (Discovery NM/CT 670 Pro, GE HealthCare, USA) (Figure 2). The background compartment was filled with distilled water, a vial-derived 869.5 MBq of ^{177}Lu, and 500 ml of 0.9% sodium chloride (NaCl, B. Braun Medical Industries Sdn. Bhd., Malaysia). The addition of NaCl solution ensured a homogeneous radioactive solution and prevented ^{177}Lu from building up on the phantom surfaces. The spheres were filled with 47.84 ml of ^{177}Lu. A tumor to background ratio (TBR) of 5:1 was achieved, with a resulting activity concentration of ^{177}Lu at 89.64 ± 2.83 MBq/ml in the spheres and 467.00 ± 14.76 MBq/ml in the background. To mimic the human lung, 20 ml of distilled water and styrofoam were used to fill the lung insert. The lung insert simulates lung tissue and features a density similar to that of the real lung tissue of a patient. This insert creates a

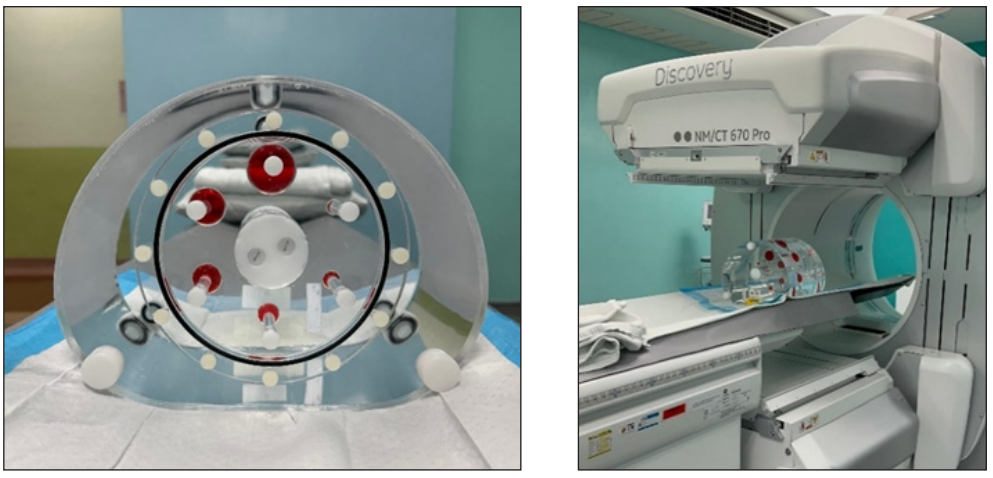

(a) (b)

Figure 2. Experimental configuration of the NEMA phantom SPECT imaging: (a) NEMA phantom filled with ^{177}Lu, and (b) acquisition geometry illustrating the alignment of the phantom with the SPECT camera
Note. NEMA = National Electrical Manufacturers Association; SPECT = Single-photon emission computed tomography

non-uniform attenuation distribution in the phantom, where attenuation and scatter properties differ markedly from those of soft tissue or bone (Mia et al., 2023). Consequently, the lung insert becomes a system for rigorously evaluating the performance and accuracy of correction algorithms under varied physiological conditions, thereby validating the robustness of image-derived quantification.

Following the SPECT acquisition, the CT scan (GE Performix Ultra CT X-ray Tube, GE HealthCare, USA) was carried out at a voltage of 120 kVp and a tube current voltage range of 10–440 mA. With the system's automated exposure control, the technology minimizes potential radiation exposure while ensuring consistent image quality throughout the body. A 20% energy window was applied to all measurements and simulations, aligned with the ^{177}Lu photopeaks at 113 keV (ranging from 101 to 124 keV) and 208 keV (ranging from 187 to 228 keV). SPECT acquisitions were conducted using a step-and-shoot approach. With a 6° angular increment and a 15-s exposure time per projection, each tomographic acquisition comprised 60 projections across 360°. The data were stored in a 128 × 128 matrix with a pixel size of 4.42 × 4.42 mm. A dose calibrator (Atomlab 500, Biodex Medical Systems, USA) has been used for the activity measurement, with each measurement repeated three times to improve the statistical accuracy of the measurement. The precision of the digital readout was 0.0001 MBq/ml. According to the manufacturer's specifications for the Atomlab 500 dose calibrator, the activity measurement accuracy is within ±3% for ^{177}Lu and similar isotopes. This value, along with an estimated volume uncertainty of about ±1% (Talukdar et al., 2019), resulted in a total measurement uncertainty of 3.16% in the reported activity concentration values.

The projected images were reconstructed using the vendor's built-in quantitative software (Q.Metrix, GE HealthCare, USA), which employs the OSEM algorithm with 2 iterations and 10 subsets. The reconstruction approach included CT-based attenuation and scatter corrections to improve quantitative accuracy. Additionally, a post-reconstruction filter, namely a Gaussian filter of 4.8 mm with FWHM, was implemented to reduce noise while preserving spatial resolution.

SPECT Imaging Using MCNP5

MCNP5, developed by Los Alamos National Laboratory (USA), was utilized in this study to model the SPECT imaging system. Figure 3 illustrates the configuration of the simulated NEMA phantom and SPECT system at different rotation angles. The transformation card in MCNP5 was used to specify each rotation angle, generating 60 projection images over 360° with a 6° angular step. The spherical inserts within the phantom, containing the activity distributions, were visualized using Visual Editor (VisEd). The phantom was positioned exactly at the center of the field-of-view (FOV) of the collimator, and simulations were carried out for ^{177}Lu under conditions identical to the experimental setup. Approximately

1.25×10^{10} and 3.35×10^{8} photons were simulated for the background and spheres, respectively, to image the phantom. The sphere simulation required an average of 75 minutes per projection, leading to a total runtime of 2,325 minutes, while the background required approximately 4.375 days per projection, accumulating to 135.625 days in total on a 3.6 GHz dual-core CPU.

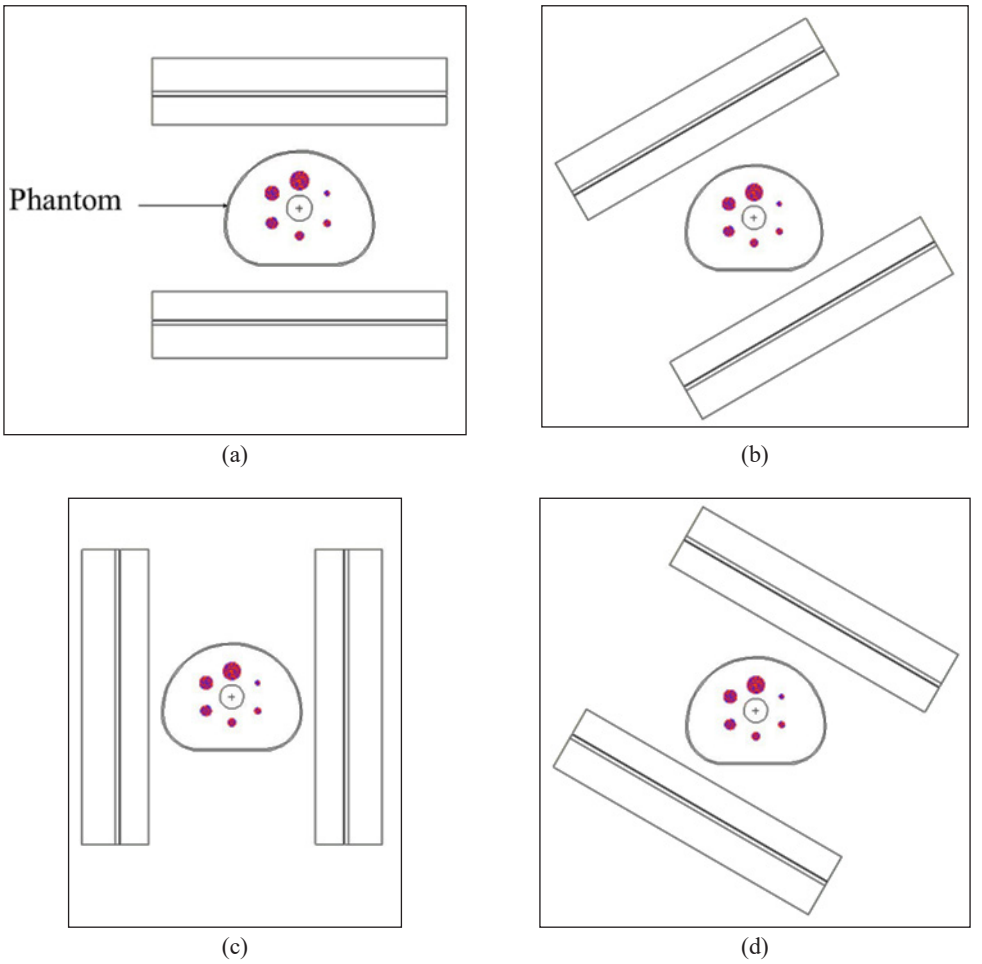

Figure 3. The geometry of the NEMA phantom and simulated SPECT system, as viewed in VisEd, is shown at different rotation angles: (a) 0°, (b) 30°, (c) 90°, and (d) 150°, with a clockwise rotation
Note. NEMA = National Electrical Manufacturers Association; SPECT = Single-photon emission computed tomography; VisEd = Visual Editor

To confine the simulation environment, a boundary was established to restrict the MCNP calculations, ensuring that any photon entering this region was excluded and forcibly terminated (Dong, 2018; Saripan, 2009). Zero importance (imp = 0) was defined for the

area beyond this boundary in MCNP5, competently removing any photon attempting to enter this area. This study acknowledges a limitation due to the unimplemented variance reduction methods.

The particle tracking (PTRAC) data generated by MCNP5 provided the core framework for the SPECT image reconstruction algorithm (Figure 4). PTRAC data, often known as list-mode data, contains essential information for photon detection, including the interaction coordinates, energy, and type of interaction. This data was created by a MATLAB algorithm to determine the energy deposited in the detector and the position of interaction. In an ideal detector, each incident photon produces a delta pulse. In practice, however, inherent variations in detector response primarily come from statistical fluctuations in the scintillation light yield. These fluctuations dominate the intrinsic resolution of the system. Although PMT gain variations contribute, their impact is secondary in scintillator-based gamma cameras. Due to these variations, the deposited energy is spread out, resulting in a Gaussian-like pulse instead of a delta pulse (Dong et al., 2018). This energy spread necessitates energy blurring in simulation to account for statistical fluctuations. A Gaussian function was applied to the energy spectrum of each detected photon, mimicking the energy spread observed in a real SPECT system to model this effect. Corresponding to the 20% window at 113 and 208 keV photopeaks, photons within the ranges of 101-124 keV and 187-228 keV were filtered. In a realistic SPECT camera, the resulting image is often blurred due to light sharing in the PMTs, causing spatial uncertainty in photon interaction positions (Dong et al., 2018). This phenomenon was modeled via position blurring, where the true interaction positions were distributed according to a 2D Gaussian distribution, leading to the formation of projections. Data necessary for image reconstruction were obtained by generating sinograms corresponding to each row of the projection image. This process is repeated for all projection angles.

The Q.Metrix application by GE HealthCare is a proprietary algorithm, precluding access to its complete internal specifications. To establish comparable reconstructions for our simulated data, an iterative reconstruction algorithm was carefully developed in MATLAB, using established quantitative SPECT reconstruction practices. The algorithm was equipped with parameters such as the number of iterations and subsets and Gaussian filter characteristics, precisely matched to those used in the experimental settings. Furthermore, attenuation and scatter corrections were incorporated into the MATLAB-based reconstruction process, comparable to the GE system. After reconstruction, the image underwent post-processing, including filtering, grayscale conversion, and transformation into uint16 format in MATLAB for improved precision before saving, ensuring compatibility with the experimental image.

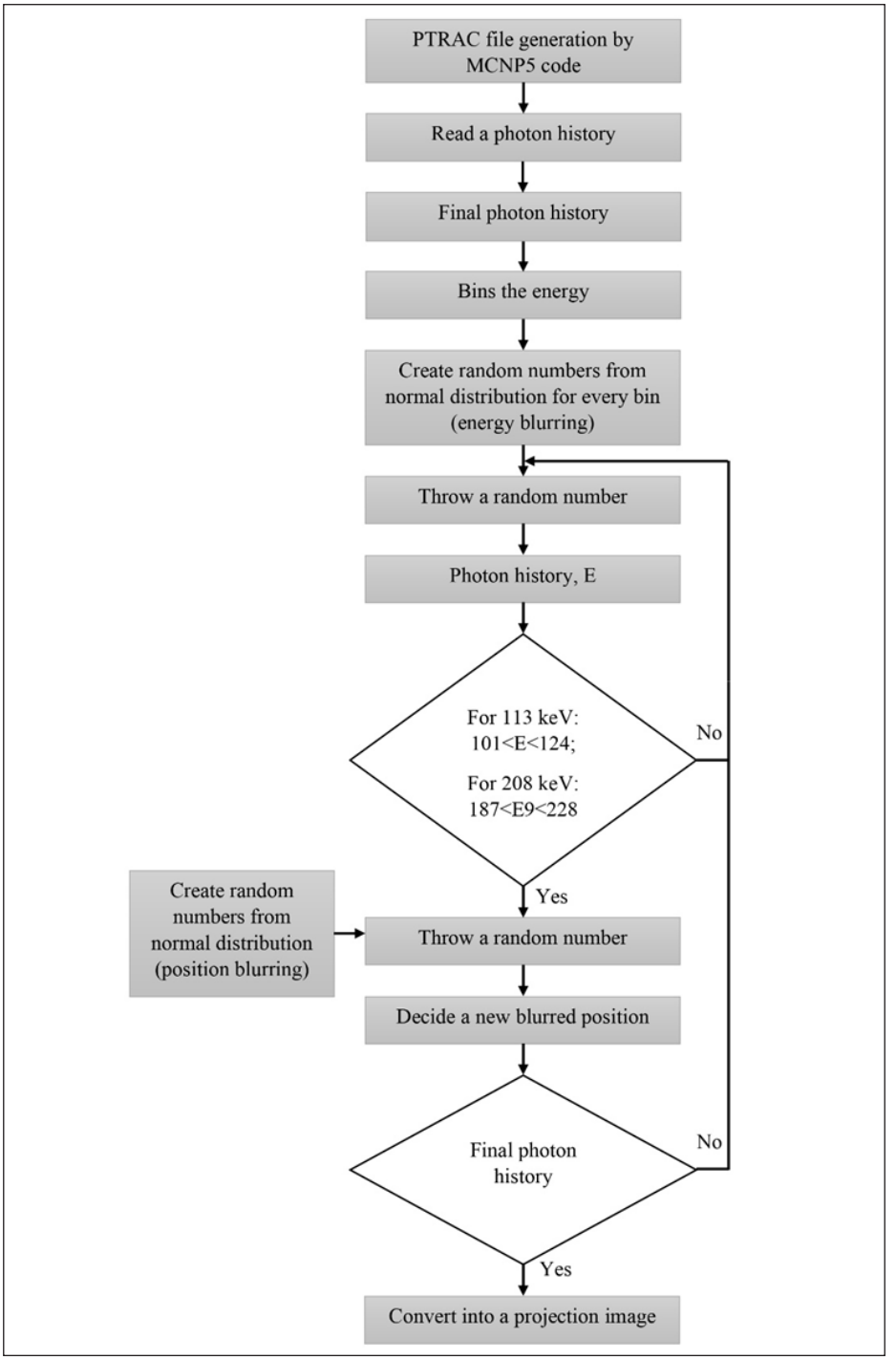

Figure 4. The SPECT image reconstruction algorithm based on PTRAC data generated by MCNP5
Note. SPECT = Single-photon emission computed tomography; PTRAC = Particle tracking; MCNP5 = Monte Carlo N-particle Transport, version 5

Verification of the MCNP5 SPECT Imaging

A set of verification criteria was used to verify the MC-simulated SPECT imaging system model through the comparison of simulated data with experimental data of the GE Discovery NM/CT 670 Pro. Verification of the MC model is necessary due to the distinct properties of the MC model. The criterion included system sensitivity, image quality, intensity profiles, and energy resolution.

Image Quality

The SSIM, which measures image quality relative to a reference image, was used in this research to evaluate the image quality. In this study, the quality of the simulated images was evaluated against the reference image, which was the experimental SPECT image. According to Roy et al. (2014) and Wang et al. (2004), SSIM is a perception-based metric that quantifies image degradation as a perceived shift in structural information. By capturing differences in contrast, brightness, and structural details, this technique assures that the evaluation is more in line with human visual perception. SSIM values vary from 0 to 1, where a value closer to 1 illustrates a high level of image similarity of simulated images in comparison with experimental images. In contrast, a value closer to 0 indicates significant structural deviation. Equation 4 illustrates the calculation of SSIM using a 3 × 3 × 3 kernel size (Rydén et al., 2021).

$$SSIM(x,y) = \frac{(2\mu_x\mu_y + C_1)(2\sigma_{xy} + C_2)}{(\mu_x^2 + \mu_y^2 + C_1)(\sigma_x^2 + \sigma_y^2 + C_2)} \quad [4]$$

where x is the reference image, y is the obtained simulated image, μ_x is the average of the reference image (x), μ_y is the average of the obtained simulated image (y), σ_x is the standard deviation of the reference image, σ_y is the standard deviation of the reference image, the standard deviation of the simulated image, and σ_{xy} is the covariance of x and y. Two variables C_1 and C_2 stabilize the division with the use of a weak denominator specified as $C_1 = (K_1L)^2, C_2 = (K_2L)^2$, where L is the dynamic range of the voxel-values, and K_1 and K_2 are default values of 0.01 and 0.03, respectively. These constants ensure numerical stability, especially in areas of low contrast.

The intensity profiles across each sphere in the experimental and simulated images were analyzed to assess the spatial distribution of the reconstructed activity in the reconstructed images. These profiles were extracted through the axial slice of each sphere along the x-axis, passing through the sphere centroid. Line profile comparisons provided insights into localized intensity variations, and Pearson's correlation coefficients were used to evaluate the overall agreement between the datasets. A high correlation coefficient between the simulated and experimental intensity distributions shows that the simulation effectively

replicates the experimental imaging, verifying the reconstruction method. Additionally, FWHM values were computed from the intensity profiles using MATLAB by identifying the width at half of the maximum intensity to further characterize the differences between simulated and experimental data.

Energy Spectra and Resolution of ^{177}Lu

Energy resolution refers to a SPECT camera's ability to distinguish between photons of different energies, specifically primary and scattered radiation (Bahreyni Toossi et al., 2010; Staelens et al., 2003; Vieira et al., 2014). The energy resolutions from the simulated and experimental setups were evaluated and compared by analyzing their corresponding energy spectra. This analysis focused on the two prominent photopeaks of ^{177}Lu, 113 and 208 keV. To quantify their energy resolutions, the corresponding photopeaks were fitted with Gaussian functions using ImageJ, an open-source software given by Fiji's public domain software (Schindelin et al., 2012). The FWHM of each photopeak was derived from the Gaussian fit and measured in energy units, being the key parameter for computing the energy resolution. The energy resolution for both photopeaks was then determined using Equation 5, which ultimately demonstrates the relationship between the FWHM and peak energy. This method guarantees a uniform measurement of spectral broadening, allowing for a comparison of the performance of the gamma camera under both simulation and experimental conditions.

$$Energy\ resolution = \frac{FWHM\ (keV)}{Energy\ (keV)} \times 100\% \quad [5]$$

RESULTS AND DISCUSSION

System Sensitivity

In this study, the system sensitivity determined experimentally was 12.12 cps/MBq, whereas the MCNP5 simulation yielded a value of 12.52 cps/MBq, reflecting a strong agreement with a deviation of approximately 3.34%. This small discrepancy, well within acceptable limits, underscores the reliability of the MC-modeled gamma camera for estimating activity concentration in ^{177}Lu SPECT imaging and demonstrates the robustness of the model for quantitative imaging. This verification is crucial for precise activity quantification in ^{177}Lu therapy monitoring, which is used for dosimetry calculations and treatment planning.

Figure 5 presents a visual and quantitative comparison of the simulated and experimental planar images of the ^{177}Lu-filled Petri dish. The intensity distributions of the simulated and experimental images showed a strong positive correlation, where Pearson's correlation coefficient demonstrates r = 0.9786. This implies that the simulated image closely resembles the intensity trends in the experimental data, demonstrating the MC model's

capacity to mimic spatial distribution patterns accurately. Lin's CCC was calculated, resulting in a value of 0.9780. According to McBride (2005), a CCC value greater than 0.95 indicates significant agreement, reinforcing that the MC model is highly accurate and precise in replicating the real planar imaging of ^{177}Lu. The simulation is a dependable tool for dosimetric and imaging studies since the near-unity Lin's CCC further verifies that it accurately and precisely preserves the absolute intensity values in addition to capturing variations in relative intensity.

(a) (b)

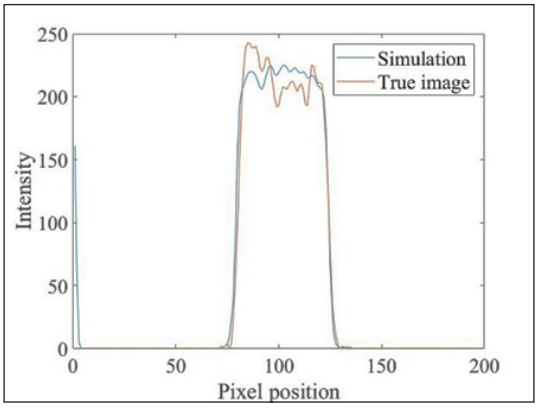

(c)

Figure 5. Comparison of Petri dish images obtained via (a) simulation in MCNP5, (b) experiment with SPECT scanner, and (c) intensity profile plotted across the center of (a) and (b)
Note. MCNP5 = Monte Carlo N-particle Transport, version 5; SPECT = Single-photon emission computed tomography

Image Quality

Figure 6 presents images reconstructed from both the MCNP5 simulation and the SPECT scanner, enabling a clear visual and quantitative comparison of the two modalities. The

SSIM was calculated to evaluate the simulated reconstruction's fidelity in comparison to the experimental data. The resulting SSIM value of 0.9348 indicates a high degree of overall structural similarity between the simulated and experimental images. This suggests that the MC model generally captures the broader structural integrity and contrast.

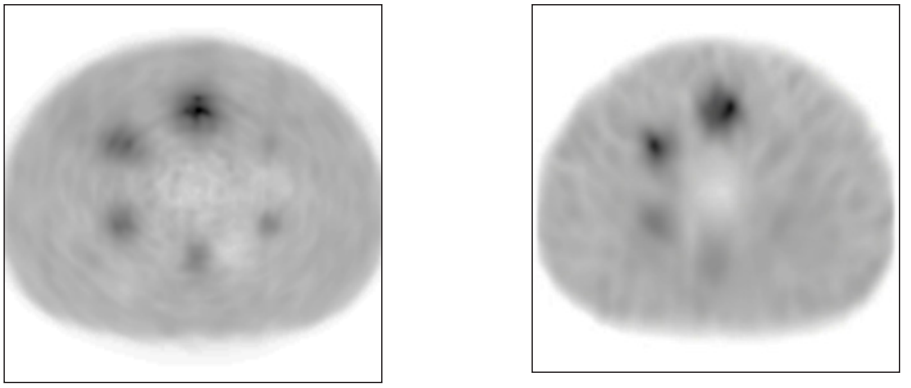

(a) (b)

Figure 6. Comparison of images of NEMA phantom determined via (a) simulation in MCNP5 and (b) experiment with SPECT scanner
Note. NEMA = National Electrical Manufacturers Association; MCNP5 = Monte Carlo N-particle Transport, version 5; SPECT = Single-photon emission computed tomography

However, a closer visual inspection of Figures 6a and 6b reveals some notable discrepancies between the experimental and simulated images that need further discussion, despite the high SSIM value indicating strong overall structural similarity. A distinct ring artifact appears in the simulated image but is not visible in the corresponding experimental image. This suggests that the simulation may not fully capture the complexities of scatter simulation or incorporate an ideal detector response that does not account for experimental system non-uniformities.

Furthermore, the smallest sphere (10 mm), which was not visible in the experimental image due to factors like noise and partial volume effects (PVEs), is clearly visible in the simulated image. This increased visibility of the smallest sphere implies that the model might not fully address the complex interactions of noise, PVEs, and limitations in spatial resolution present in the experimental setup. As a result, the simulation may overestimate its ability to precisely predict the detectability limits of small lesions or provide accurate quantitative results for these volumes. This could lead to inflated RCs for very small volumes.

Although the high SSIM value indicates an overall structural similarity, it is crucial to understand that this metric may not capture the clinical significance of specific localized artifacts or accurately reflect the system's true detectability limits, as shown by the

visual findings. Future refinements of the MCNP5 model will focus on addressing these specific discrepancies by refining noise models to better reflect experimental systems or implementing more advanced scatter correction algorithms within the simulation environment. This iterative refinement is vital for improving the model's fidelity and enhancing its applicability for accurate and precise quantitative analysis and patient-specific dosimetry.

Figure 7 presents a comparative analysis of intensity profiles for each sphere in the experimental and simulated images. Pearson's correlation coefficients for all spheres were computed to objectively evaluate the agreement between the two datasets. The coefficients for the spheres of sizes 13, 17, 22, 28, and 37 mm were 0.9037, 0.9515, 0.9592, 0.9626, and 0.9882, respectively. As the size of the sphere increases, these results display a progressively stronger positive correlation, suggesting that the simulated and experimental intensity distributions agree better for larger volumes. The largest sphere (37 mm) showed the highest correlation (0.9882), indicating that the simulation reproduces the activity distribution in larger spheres with minimal variation from experimental results.

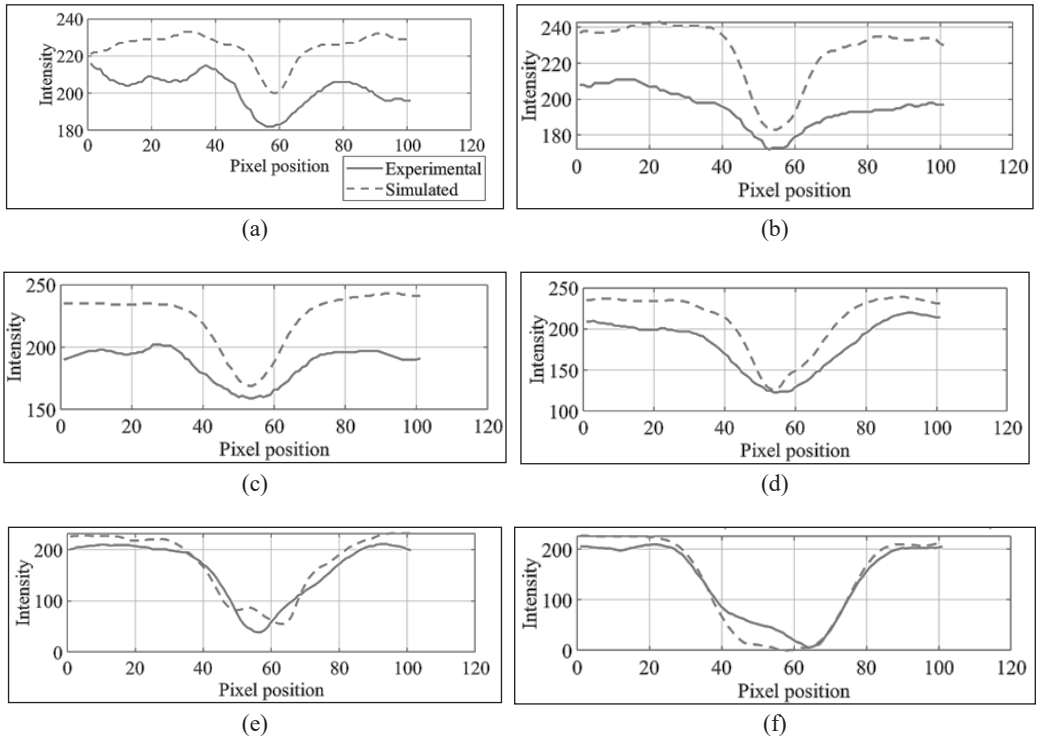

Figure 7. Comparison of intensity profiles across each sphere: (a) 10 mm, (b) 13 mm, (c) 17 mm, (d) 22 mm, (e) 28 mm, and (f) 37 mm, in experimental and simulated NEMA phantom images
Note. NEMA = National Electrical Manufacturers Association

The smallest sphere (10 mm) has a lower correlation coefficient of 0.7509. This reduced correlation highlights challenges in modeling small volume quantification. PVEs, arising from the finite spatial resolution of the gamma camera, become more pronounced as the sphere size decreases. This results in an underestimation of activity in the true volume (and thus the estimated absorbed dose) and an inaccurate volume estimation (Di Domenico et al., 2023). Although PVE affects both experimental and simulated data to a similar extent, the simulation seems to underestimate its impact. This observed discrepancy between our simulation and experiment likely stems from an overly optimistic spatial resolution model in the simulation and insufficient noise modeling. For instance, the simulation might be underestimating the intrinsic resolution degradation of the detector, or the noise characteristics of the simulated images may not fully reflect the complexities of experimental noise, thereby leading to a less pronounced PVE than observed experimentally, and artificially enhanced detectability in the simulated images.

Additionally, statistical noise, inherent to low photon counts, can significantly impact image quantification, particularly for smaller spheres (Allangba et al., 2023). Lower photon counts result in higher variability in activity reconstructions, increasing the differences between simulated and experimental images. The differences are especially notable in small volumes, where a decreased signal-to-noise ratio (SNR) complicates precise activity quantification. MC simulations often rely on idealized photon transport models that lack the exact noise characteristics of real-world imaging systems. Therefore, experimental data may show higher variations due to the statistical noise and instrumentation-related issues. This discovery is consistent with prior research, which has demonstrated that larger structures have less blurring and are less vulnerable to photon count limitations, resulting in improved quantitative accuracy (Ljungberg & Sjögreen-Gleisner, 2011; Sarrut et al., 2021; Zaidi, 1999).

Table 3 provides a quantitative summary of the FWHM values computed for each sphere in experimental and simulated data. Notably, the larger spheres (37 and 28 mm) showed excellent agreement between the experimental and simulated FWHM values, with percent differences of only 1.37 and 0.25%, respectively. For these larger spheres, the experimental and simulated intensity profiles also demonstrated good qualitative agreement in terms of overall dip shape and approximate depth.

In contrast, a pronounced discrepancy was observed for the smaller spheres (22, 17, and 13 mm). The simulated FWHM values for these spheres were consistently and significantly lower than the experimental FWHM values, implying a more idealized resolution in the simulation. Evidently, the simulated intensity profiles consistently exhibited deeper and sharper intensity dips compared to the progressively shallower and broader experimental profiles. This FWHM discrepancy was most pronounced for the 13 mm sphere, with a percent difference of 39.06%.

Table 3
FWHM values for spheres in experimental and simulated NEMA phantom images

Sphere diameter (mm)	Experimental FWHM (mm)	Simulated FWHM (mm)	Percent difference (%)
10.00	15.19	16.39	7.94
13.00	27.97	17.05	39.06
17.00	32.06	20.12	37.26
22.00	28.96	22.21	23.29
28.00	27.50	27.57	0.25
37.00	36.46	36.96	1.37

Note. FWHM = Full width at half maximum; NEMA = National Electrical Manufacturers Association

This trend reflects the nonlinear recovery behaviour in SPECT imaging and the pronounced impact of PVEs on medium-sized spheres. A previous study has shown that medium-sized spheres (13, 17, and 22 mm) are most affected by PVEs, with correction methods improving quantification by approximately 70%, while larger spheres (28 and 37 mm) exhibit minimal underestimation (Allangba et al., 2023). For the smallest sphere (10 mm), the interpretation of FWHM is complex due to its proximity to the system's intrinsic resolution limit, leading to increased noise sensitivity and fitting variability in the FWHM estimation. Furthermore, while simulated data generally show isotropic blurring (similar FWHM in x and y), experimental results reveal anisotropic effects, suggesting real-world asymmetries in the imaging system. A recent study also reported that filtering post-reconstruction images can increase the degree of negative bias in smaller objects while removing positive noise-induced bias in larger spheres of unfiltered images (Dickson et al., 2022).

Energy Resolution of ^{177}Lu

Figure 8 shows the energy spectrum from the SPECT simulation model and SPECT imaging, reflecting the energies of photons detected by the gamma camera, which are impacted by the physical properties of the radionuclide and detector. Prior to energy and position blurring, the energy spectrum exhibits discrete peaks corresponding to the energies of the emitted photons from ^{177}Lu, peaks at 113 keV and 208 keV (Figure 8a).

Gaussian energy blurring was implemented to account for system imperfections and random fluctuations in photon detection, thereby imitating real SPECT imaging (Musarudin et al., 2015). A sigma value of 1.6 was used for this Gaussian blurring applied during the iterative reconstruction process. This resulted in a smear, broadening, and Gaussian-shaped spectrum of the photopeaks (Figure 8b). While this blurring method accurately replicates the general broadening and shape of the peaks, the resulting spectrum qualitatively corresponds to the experimental energy spectrum (Figure 8c).

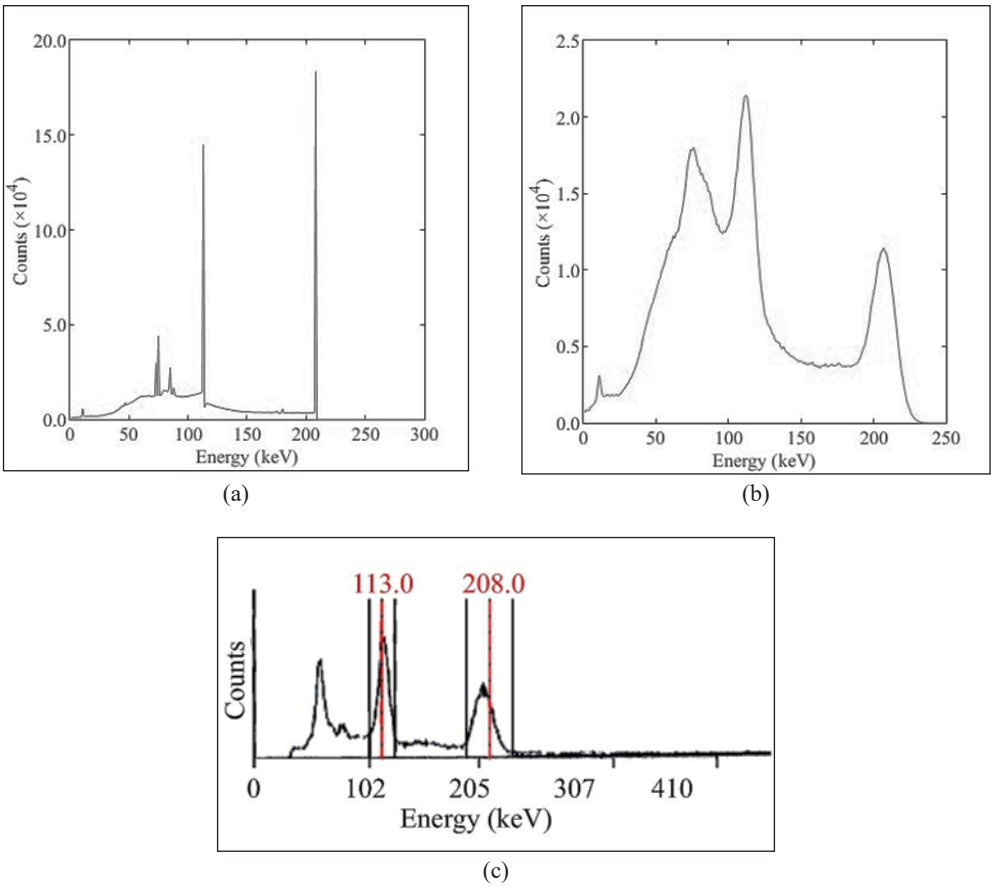

Figure 8. Simulated and experimental energy spectra: (a) and (b) represent the simulated energy spectrum before and after applying Gaussian energy blurring, respectively, and (c) presents the experimental energy spectrum
Note. Red straight lines indicate the peak energies of lutetium-177 (^{177}Lu)

The FWHM of the photopeaks was utilized to compute simulated energy resolution. The simulated energy resolution at 113 and 208 keV was 16.28 and 15.69%, respectively. This difference arises due to the energy-dependent nature of SPECT imaging detection. Lower energies, at 113 keV, typically exhibit poorer resolution compared to higher energies like 208 keV, primarily due to greater statistical fluctuations in events within the imaging chain at lower energies, where fewer photons are produced in the scintillator, resulting in broader peaks (White, 2015). The above-mentioned explains the variation in the number of simulated counts for the 113 and 208 photopeaks.

As shown in Figure 8c, the overall shape and major peaks of the simulated energy spectrum are consistent with the experimental range. However, the 208 keV peak aligns better with the experimental data compared to the 113 keV peak, where the simulated width appears wider than in the experimental data. This difference suggests that, while

the Gaussian blurring adequately models the broadening, it may not effectively represent the detector's energy response across the energy spectrum for isotopes emitting multiple energies. Previous studies have reported similar outcomes, highlighting that energy blurring does not always achieve full agreement across the entire energy spectrum for isotopes with multiple emissions (Assié et al., 2005; Morphis et al., 2021; Robinson et al., 2016). Future research on the MCNP5 model will attempt to optimize the energy blurring parameters to achieve a more precise match for all photopeaks, particularly for lower energy outputs.

CONCLUSION

This study presents a validated MCNP5 model of the GE HealthCare Discovery NM/CT 670 Pro SPECT gamma camera for ^{177}Lu SPECT imaging. The MCNP5 modeled gamma camera was systematically validated for ^{177}Lu imaging by assessing several key performance metrics, including system sensitivity, image quality, intensity profiles, and energy resolution. The results demonstrated strong agreement between the simulated and experimental system sensitivities (3.34% variation), a high SSIM value (0.9348) indicating high overall structural resemblance, and excellent correlation coefficients across larger structures (0.9882 for the 37 mm sphere and 0.9626 for the 28 mm sphere). This study thus confirms that the MCNP5 model of the SPECT scanner, along with all subsequent post-simulation programs, effectively replicates the conditions of real-world SPECT scanning for general image characteristics and larger structures.

However, the MC model revealed limitations when simulating smaller structures, particularly those under 28 mm in diameter, including underestimated blurring and overestimated contrast. The detectability of the smallest sphere (10 mm) with a lower correlation coefficient (0.7509) further highlights the need for improvement in the modeling of underlying physical interactions.

Despite these discrepancies, it is evident that MCNP5 can successfully emulate the clinical Discovery NM/CT 670 Pro, making it a reliable tool for modeling planar and SPECT imaging for ^{177}Lu, particularly for studies involving larger structures and general image characteristics. This successful validation enhances confidence in MCNP5's potential for future research. Continued refinement, focusing on optimizing noise models, detector response, and scatter simulations, is crucial to enhance the model's fidelity further. It emphasizes its greater clinical applicability, which could enhance diagnostic accuracy and activity quantification in nuclear medicine.

ACKNOWLEDGMENTS

The authors extend their sincere gratitude to the Ministry of Higher Education Malaysia for supporting this research through the Fundamental Research Grant Scheme with project code FRGS/1/2021/SKK06/USM/03/1.

REFERENCES

Allangba, K. N. P. G., Koutouan, A. K., Giuliano, A., Traoré, Z., & Traino, A. (2023). Partial Volume Effect (PVE) correction in Single Photon Emission Computed Tomography (SPECT) Imaging. *Radiation Science and Technology*, *9*(3), 26–35. https://doi.org/10.11648/j.rst.20230903.11

Asmi, H., Bentayeb, F., Bouzekraoui, Y., Bonutti, F., & Douama, S. (2020). Energy window and collimator optimization in lutetium-177 single-photon emission computed tomography imaging using Monte Carlo simulation. *Indian Journal of Nuclear Medicine*, *35*(1), 36–39. https://doi.org/10.4103/ijnm.IJNM_121_19

Assié, K., Gardin, I., Véra, P., & Buvat, I. (2005). Validation of the Monte Carlo simulator GATE for indium-111 imaging. *Physics in Medicine and Biology*, *50*(13), 3113. https://doi.org/10.1088/0031-9155/50/13/010

Bahnamiri, S. B. (2015). Investigation of collimator influential parameter on SPECT image quality: A Monte Carlo study. *Journal of Biomedical Physics and Engineering*, *5*(1), 39–48.

Bahreyni Toossi, M. T., Islamian, J. P., Momennezhad, M., Ljungberg, M., & Naseri, S. H. (2010). SIMIND Monte Carlo simulation of a single photon emission CT. *Journal of Medical Physics*, *35*(1), 42–47. https://doi.org/10.4103/0971-6203.55967

Bodei, L., Cremonesi, M., Grana, C. M., Fazio, N., Iodice, S., Baio, S. M., Bartolomei, M., Lombardo, D., Ferrari, M. E., Sansovini, M., Chinol, M., & Paganelli, G. (2011). Peptide receptor radionuclide therapy with ^{177}Lu-DOTATATE: The IEO phase I-II study. *European Journal of Nuclear Medicine and Molecular Imaging*, *38*, 2125–2135. https://doi.org/10.1007/s00259-011-1902-1

Bouchareb, Y., AlSaadi, A., Zabah, J., Jain, A., Al-Jabri, A., Phiri, P., Shi, J. Q., Delanerolle, G., & Sirasanagandla, S. R. (2024). Technological advances in SPECT and SPECT/CT imaging. *Diagnostics*, *14*(13), 1431. https://doi.org/10.3390/diagnostics14131431

Bui, M. H. H. H., Robert, A., Badel, J. N., Kvassheim, M., Stokke, C., Rit, S., & Etxebeste, A. (2023). Validation of a model of the Symbia Intevo Bold SPECT scanner for Monte Carlo simulations. In IEEE *Nuclear Science Symposium and Medical Imaging Conference* (p. 1). IEEE. https://doi.org/10.1109/NSSMICRTSD49126.2023.10338340

D'Arienzo, M., Cazzato, M., Cozzella, M. L., Cox, M., D'Andrea, M., Fazio, A., Fenwick, A., Iaccarino, G., Johansson, L., Strigari, L., Ungania, S., & De Felice, P. (2016). Gamma camera calibration and validation for quantitative SPECT imaging with ^{177}Lu. *Applied Radiation and Isotopes*, *112*, 156–164. https://doi.org/10.1016/j.apradiso.2016.03.007

De Vries, D. J., Moore, S. C., Zimmerman, R. E., Mueller, S. P., Friedland, B., & Lanza, R. C. (1990). Development and validation of a Monte Carlo simulation of photon transport in an Anger camera. *IEEE Transactions on Medical Imaging*, *9*(4), 430–438. https://doi.org/10.1109/42.61758

Di Domenico, G., Di Biaso, S., Longo, L., Turra, A., Tonini, E., Longo, M. C., Uccelli, L., & Bartolomei, M. (2023). Validation of ^{99m}Tc and ^{177}Lu quantification parameters for a Monte Carlo modelled gamma camera. *EJNMMI Physics*, *10*, 27. https://doi.org/10.1186/s40658-023-00547-6

Dickson, J. C., Armstrong, I. S., Gabiña, P. M., Denis-Bacelar, A. M., Krizsan, A. K., Gear, J. M., Van den Wyngaert, T., de Geus-Oei, L.-F., & Herrmann, K. (2022). EANM practice guideline for quantitative SPECT-CT. *European Journal of Nuclear Medicine and Molecular Imaging*, *50*, 980–995. https://doi.org/10.1007/s00259-022-06028-9

Dong, X., Saripan, M. I., Mahmud, R., Mashohor, S., & Wang, A. (2018). Characterization of SIEMENS Symbia T SPECT camera in Monte Carlo simulation environment. *Pakistan Journal of Nuclear Medicine*, *8*(1), 18–26. https://doi.org/10.24911/pjnmed.175-1540569779

Ejeh, J. E., van Staden, J. A., & du Raan, H. (2019). Validation of SIMIND Monte Carlo simulation software for modelling a Siemens Symbia T SPECT scintillation camera. In L. Lhotska, L. Sukupova, I. Lacković, & G. S. Ibbott (Eds.), *World Congress on Medical Physics and Biomedical Engineering 2018* (pp. 573-576). Springer. https://doi.org/10.1007/978-981-10-9035-6_106

Ezziddin, S., Khalaf, F., Vanezi, M., Haslerud, T., Mayer, K., Al Zreiqat, A., Willinek, W., Biersack, H.-J., & Sabet, A. (2014). Outcome of peptide receptor radionuclide therapy with ^{177}Lu-octreotate in advanced grade 1/2 pancreatic neuroendocrine tumours. *European Journal of Nuclear Medicine and Molecular Imaging*, *41*, 925–933. https://doi.org/10.1007/s00259-013-2677-3

GE HealthCare. (n.d.). *Discovery NM/CT 670 Pro: Data sheet*. https://www.probomedical.com/wp-content/uploads/2024/09/GE-Discovery-670.pdf

Ilan, E., Sandström, M., Wassberg, C., Sundin, A., Garske-Román, U., Eriksson, B., Granberg, D., & Lubberink, M. (2015). Dose response of pancreatic neuroendocrine tumors treated with peptide receptor radionuclide therapy using ^{177}Lu-DOTATATE. *Journal of Nuclear Medicine*, *56*(2), 177–182. https://doi.org/10.2967/jnumed.114.148437

Ljungberg, M., & Sjögreen-Gleisner, K. (2011). The accuracy of absorbed dose estimates in tumours determined by quantitative SPECT: A Monte Carlo study. *Acta Oncologica*, *50*(6), 981–989. https://doi.org/10.3109/0284186x.2011.584559

McBride, G. B. (2005). *A proposal for strength-of-agreement criteria for Lin's concordance correlation coefficient*. https://www.medcalc.org/download/pdf/McBride2005.pdf

Mia, M. S., Hossain, M. N., Biman, T. A., & Kabir, M. F. F. (2023). Performance evaluation of the GE Discovery IQ PET/CT system according to the NEMA NU2-2012 standard. *Bangladesh Journal of Physics*, *30*(2), 57–67. https://doi.org/10.3329/bjphy.v30i2.68384

Mishra, A. (2024). Gamma Cameras: Exploring the technology, applications, and future prospects. *American Academic Scientific Research Journal for Engineering, Technology, and Sciences*, *98*(1), 296–308.

Morphis, M., van Staden, J. A., du Raan, H., & Ljungberg, M. (2021). Modelling of energy-dependent spectral resolution for SPECT Monte Carlo simulations using SIMIND. *Heliyon*, *7*(2), e06097. https://doi.org/10.1016/j.heliyon.2021.e06097

Morthy, P. (2025). Optimization of the acquisition and reconstruction protocol for quantitative ^{177}Lu SPECT/CT. *Australasian College of Physical Scientists and Engineers in Medicine*. https://doi.org/10.1007/s13246-024-01502-0

Morthy, P., Musarudin, M., Ab Shukor, N. S., Said, M. A., Xianling, D., & Saripan, M. I. (2025). Accuracy of ^{177}Lu activity quantification using MCNP5-modeled SPECT imaging. *Applied Radiation and Isotopes*, *220*, 111786. https://doi.org/10.1016/j.apradiso.2025.111786

Musarudin, M., Saripan, M. I., Mashohor, S., Saad, W. H. M., Hashim, S., & Nordin, A. J. (2015). Validation of a clinical PET scanner using Monte Carlo simulation code: MCNP5. In *8th EUROSIM Congress on Modelling and Simulation* (pp. 36–41). IEEE. https://doi.org/10.1109/EUROSIM.2013.16

Nakanishi, K., Fujita, N., Abe, S., Nishii, R., & Kato, K. (2024). A simple method to shorten the apparent dead time in the dosimetry of Lu-177 for targeted radionuclide therapy using a gamma camera. *Physica Medica*, *119*, 103298. https://doi.org/10.1016/j.ejmp.2024.103298

Paganelli, G., Sansovini, M., Ambrosetti, A., Severi, S., Monti, M., Scarpi, E., Donati, C., Ianniello, A., Matteucci, F., & Amadori, D. (2014). 177 Lu-Dota-octreotate radionuclide therapy of advanced gastrointestinal neuroendocrine tumors: Results from a phase II study. *European Journal of Nuclear Medicine and Molecular Imaging*, *41*, 1845–1851. https://doi.org/10.1007/s00259-014-2735-5

Pells, S., Cullen, D. M., Deidda, D., Denis-Bacelar, A. M., Fenwick, A., Ferreira, K. M., Hamilton, D., Heetun, W., Julyan, P., Needham, G., Pietras, B., Price, E., Scuffham, J., Tipping, J., & Robinson, A. P. (2023). Quantitative validation of Monte Carlo SPECT simulation: Application to a Mediso AnyScan GATE simulation. *EJNMMI Physics*, *10*, 60. https://doi.org/10.1186/s40658-023-00581-4

Ramonaheng, K., van Staden, J. A., & du Raan, H. (2020). Validation of a Monte Carlo modelled gamma camera for Lutetium-177 imaging. *Applied Radiation and Isotopes*, *163*, 109200. https://doi.org/10.1016/j.apradiso.2020.109200

Robinson, A. P., Tipping, J., Cullen, D. M., & Hamilton, D. (2016). The influence of triple energy window scatter correction on activity quantification for ^{177}Lu molecular radiotherapy. *Physics in Medicine and Biology*, *61*(14), 5107–5127. https://doi.org/10.1088/0031-9155/61/14/5107

Romer, A., Seiler, D., Marincek, N., Brunner, P., Koller, M. T., Ng, Q. K. T., Maecke, H. R., Müller-Brand, J., Rochlitz, C., Briel, M., Schindler, C., & Walter, M. A. (2014). Somatostatin-based radiopeptide therapy with [^{177}Lu-DOTA]-TOC versus [^{90}Y-DOTA]-TOC in neuroendocrine tumours. *European Journal of Nuclear Medicine and Molecular Imaging*, *41*, 214–222. https://doi.org/10.1007/s00259-013-2559-8

Roy, P., Dutta, S., Dey, N., Dey, G., Chakraborty, S., & Ray, R. (2014). Adaptive thresholding: A comparative study. In *International Conference on Control, Instrumentation, Communication and Computational Technologies* (pp. 1182–1186). IEEE. https://doi.org/10.1109/ICCICCT.2014.6993140

Rydén, T., Van Essen, M., Marin, I., Svensson, J., & Bernhardt, P. (2021). Deep-learning generation of synthetic intermediate projections improves ^{177}Lu SPECT images reconstructed with sparsely acquired projections. *Journal of Nuclear Medicine*, *62*(4), 528–535. https://doi.org/10.2967/jnumed.120.245548

Saripan, M. I., Mohd Saad, W. H., Hashim, S., Mahmud, R., Nordin, A. J., & Mahdi, M. A. (2009). Monte Carlo simulation on breast cancer detection using wire mesh collimator gamma camera. *IEEE Transactions on Nuclear Science*, *56*(3), 1321–1324. https://doi.org/10.1109/TNS.2008.2012058

Sarrut, D., Etxebeste, A., Muñoz, E., Krah, N., & Létang, J. M. (2021). Artificial intelligence for Monte Carlo simulation in medical physics. *Frontiers in Physics*, *9*, 738112. https://doi.org/10.3389/fphy.2021.738112

Schindelin, J., Arganda-Carreras, I., Frise, E., Kaynig, V., Longair, M., Pietzsch, T., Preibisch, S., Rueden, C., Saalfeld, S., Schmid, B., Tinevez, J.-Y., White, D. J., Hartenstein, V., Eliceiri, K., Tomancak, P., & Cardona, A. (2012). Fiji: An open-source platform for biological-image analysis. *Nature Methods*, *9*, 676–682. https://doi.org/10.1038/nmeth.2019

Seo, Y., Mari, C., & Hasegawa, B. H. (2008). Technological development and advances in single-photon emission computed tomography/computed tomography. *Seminars in Nuclear Medicine*, *38*(3), 177–198. https://doi.org/10.1053/j.semnuclmed.2008.01.001

Staelens, S., Strul, D., Santin, G., Vandenberghe, S., Koole, M., Asseler, Y. D., Lemahieu, I., & Van de Walle, R. (2003). Monte Carlo simulations of a scintillation camera using GATE: Validation and application modelling. *Physics in Medicine and Biology*, *48*(18), 3021–3042. https://doi.org/10.1088/0031-9155/48/18/305

Talukdar, M., Dewhirst, H., & Paulsen, A. (2019). Assaying lutetium 177 in a dose calibrator. *Journal of Nuclear Medicine*, *60*(supplement 1), 2080.

van der Zwan, W. A., Bodei, L., Mueller-Brand, J., de Herder, W. W., Kvols, L. K., & Kwekkeboom, D. J. (2015). GEP–NETs UPDATE: Radionuclide therapy in neuroendocrine tumors. *European Journal of Endocrinology*, *172*(1), R1–R8. https://doi.org/10.1530/EJE-14-0488

Vieira, L., Vaz, T. F., Costa, D. C., & Almeida, P. (2014). Monte Carlo simulation of the basic features of the GE Millennium MG single photon emission computed tomography gamma camera. *Revista Española De Medicina Nuclear E Imagen Molecular*, *33*(1), 6–13. https://doi.org/10.1016/j.remn.2013.03.009

Wang, Z., Bovik, A. C., Sheikh, H. R., & Simoncelli, E. P. (2004). Image quality assessment: From error visibility to structural similarity. *IEEE Transactions on Image Processing*, *13*(4), 600–612. https://doi.org/10.1109/TIP.2003.819861

White, S. L. (2015). *Basic principles of gamma camera imaging and quality control*. https://amos3.aapm.org/abstracts/pdf/99-30890-359478-110770.pdf

Zaidi, H. (1999). Relevance of accurate Monte Carlo modeling in nuclear medical imaging. *Medical Physics*, *26*(4), 574–608. https://doi.org/10.1118/1.598559